ISSN 1063-7761, Journal of Experimental and Theoretical Physics, 2021, Vol. 132, No. 1, pp. 94–101. © Pleiades Publishing, Inc., 2021.
Russian Text © The Author(s), 2021, published in Zhurnal Eksperimental'noi i Teoreticheskoi Fiziki, 2021, Vol. 159, No. 1, pp. 111–119.

ORDER, DISORDER, AND PHASE TRANSITION IN CONDENSED SYSTEM

Phonon Spectroscopy of the Schottky-Like Low-Energy Paramagnetic Excitations in Garnet Solid Solution Crystals

A. V. Taranov[a,*], E. N. Khazanov[a,], and E. V. Charnaya[b]**

[a] *Kotel'nikov Institute of Radio Engineering and Electronics, Russian Academy of Sciences, Moscow, 125009 Russia*
[b] *St. Petersburg State University, St. Petersburg, 199034 Russia*
**e-mail: taranov@cplire.ru*
***e-mail: khazanov@cplire.ru*

Received July 16, 2020; revised August 20, 2020; accepted August 30, 2020

Abstract—The interaction of weakly nonequilibrium phonons with the low-energy paramagnetic excitations of the rare-earth ions of the yttrium series in rare-earth garnet solid solutions is studied at liquid-helium temperatures. The interaction of nonequilibrium phonons with the low-energy excitations of Ho^{3+} and Tb^{3+}, which are caused by local electric fields in a crystal lattice, is experimentally investigated. In the row of Kraemrs ions (where the nature of low-energy excitations is caused by the splitting of the ground level of a paramagnetic ion due to the local magnetic fields of neighboring ions), interaction in the nonequilibrium phonon–low-energy excitation system is only detected in the Er-containing solid solutions and is absent in the structures containing Gd^{3+}, Dy^{3+}, and Yb^{3+} rare-earth ions. In the two-level system model, the efficiency of interaction and the transport characteristics of thermal phonons are shown to depend on the type of rare-earth ion, the energy and spectral features of two-level systems, the moments of electrons in the 4*f* shell, and spin–lattice relaxation.

DOI: 10.1134/S1063776121010052

INTRODUCTION

The presence of rare-earth (RE) metal ions in the structure of solid insulators causes a wide range of their physical properties and methods of their investigation. At low temperatures, magnetically ordered phases can form [1], various magnetic-field-induced states appear [2–4], and Schottky-like excitations (which determine the low-temperature thermodynamic and kinetic characteristics of thermal phonons) appear [5]. The main methods used to study the specific features of RE ions in the structures of various materials are EPR and NMR [6, 7]. An analysis of the transport characteristics of phonons at liquid-helium temperatures makes it possible to investigate the nature of low-energy vibrational states and the contributions of various mechanisms to thermal-phonon scattering [8] and to find a relation between the kinetic characteristics of phonons during the nonstationary process of their propagation to the data of stationary low-temperature measurements of heat capacity [5].

The diversity of the properties of paramagnetic ions is caused by the electronic structure of the 4*f* inner shell and exhibits a certain function of the degree of its filling [6]. A crystal field partly of fully lifts the degeneracy of the ground level of a magnetic ion by splitting each term into a multiplet of Stark levels. Dynamic electric fields can excite transitions between Stark levels, which serves as the basis for creating laser media over a wide energy range [9]. The high magnetocaloric moments of the materials containing paramagnetic ion impurities make it possible to use them in glassy carbon refrigerators [10, 11].

The total momentum of an electron is only due to the total spin moment of a paramagnetic ion, and the contribution of orbital moment is absent. Therefore, only weak interactions with static (weak Stark splitting) and dynamic (weak relation to lattice vibrations, slow spin–lattice relaxation) electric fields are possible in this case. As a rule, the Stark level energy exceeds several tens and hundreds of kelvins. The splitting of Kramers doublets in a zero magnetic field is at most 13 K. It is Kramers ions and Stark levels with an energy lower than 10 K that mainly determine the thermodynamic and kinetic characteristics of phonons at liquid-helium temperatures.

The purpose of this work is to analyze the thermodynamic and transport characteristics of thermal phonons in dielectric solid solutions with REM impurities of the yttrium series at liquid-helium temperatures.

We use the term Schottky-like excitations, since, in contrast to the classical Schottky anomaly in a zero magnetic field, the nature of the low-temperature excitations under study is caused by the local magnetic

fields of the nearest paramagnetic ions, which bring about splitting of a Kramers doublet.

EXPERIMENTAL

We experimentally study the transport characteristics of nonequilibrium phonons (NPs) and heat capacity $C(T)$ at liquid-helium temperatures in solid-solution single crystals $Y_{3-x}Re_xAl_5O_{12}$ (YAG:Re; Re = Er, Gd, Ho, Dy, Tb), $Tm_{3-x}Er_xAl_5O_{12}$ (TmAG:Er), $Gd_3Ga_5O_{12}$ (GGG), and GGG:Er.

The heat capacity $C(T)$ of samples was measured with a PPMS-9+Ever Cool-II (Quantum Design) measurement setup in the temperature range 1.9–220 K.

The technique of measuring the kinetic characteristics of phonons consists in heating of a metal (Au) film on one of the sample ends by short current pulses ($t < 100$ ns) and in detecting a signal by a broadband superconducting bolometer based on an Sn film on the opposite end face of the sample. The sample size in the heat pulse propagation direction was changed from 0.1 to 1 cm. The studies were carried out in the temperature range 2.2–3.8 K. During measurements, samples were fully submerged in liquid helium, which provided effective heat removal from an injector film and low inertia of the bolometer. Phonon injector temperature T_h was higher than thermostat temperature T_0 by $\Delta T = T_h - T_0 \ll T_0$; that is, the phonons were weakly nonequilibrium and the samples had the thermostat temperature. The pulse power released in the injector film did not exceed 0.1 W/mm^2. At the given degree of doping, more than 5% NPs propagated in the diffusion mode. In the general case, $t_m(T)$, i.e., the time it takes for the bolometer to detect signal maximum $S(t)$, is the quantity to be measured in the presence of a few NP scattering mechanisms. The signals detected by the bolometer were measured within the linear segment of the bolometer characteristic. For elastic scattering, the detected signals were well described by the solution to the nonstationary diffusion equation

$$\Delta T(t) \propto t^{-1/2} \exp\left(-\frac{L^2}{4D_0(T)t}\right) \quad (1)$$

("flat" source), were ΔT is the difference between the bolometer-detected temperature and the thermostat temperature, L is the sample length along the NP propagation direction, ad D_0 is the diffusion coefficient. In the case of only elastic scattering, the time $t_{m0}(T)$ of arrival of the maximum of a diffusion signal is unambiguously related to the diffusion coefficient as

$$t_{m0}(T) = \frac{L^2}{2D_0(T)},$$

where $D_0 = v^2\tau_0(\omega)/3$, v is the polarization-averaged velocity of sound, and $\tau_0(\omega) \propto T^{-4}$ is the time of elastic NP scattering. With this approach, we can study the temperature dependences of the kinetic characteristics in the diffusion mode by changing the thermostat temperature. At liquid-helium temperatures ($T_0 < 4$ K), the inelastic phonon–phonon interactions caused by lattice anharmonicity are unlikely in relatively short samples. The experimental measurements [12] and theoretical estimates give about 10^{-2} s. Therefore, the efficiency of NP scattering under the experimental conditions was mainly determined by elastic phonon scattering, which was associated with the mutual substitution of RE ions at the dodecahedral c sites of the solid-solution lattice [13] and with low-energy excitations. The temperature range of measurements was bounded below by the λ point of helium and bounded above by the superconducting film temperature in the bolometer. The specific features of the experiment, which are related to an increase in the injector temperature (increase in the NP energy) and to the specific features of transport caused by a combination of effective elastic scattering and the inelastic scattering due to lattice anharmonicity, were considered in [14]. The insignificant heating of the phonon injector ($\Delta T = 0.1$–0.2 K), the short observation time (small sample size), and the high RE ion concentration used in this work were intended to exclude the anharmonicity-induced phonon–phonon interactions in order to analyze the NP–two-level system (TLS) interactions.

The presence of low-energy Schottky-like excitations in the temperature range under study can contribute to the scattering of thermal pulse phonons. The phonon range length (l_R) and time (τ_R) in the diffusion mode of relatively inelastic interaction with low-energy excitations were considered in [15] and can be estimated from the expression $l_R \approx v\sqrt{\tau_0(\omega)\tau_R(\omega)}$ [16] or

$$l_R \approx \sqrt{D_0(\omega)\tau_R(\omega)}. \quad (2)$$

This process means that, when traveling distance l_R, a phonon of frequency ω can be multiply elastically scattered before interaction with TLS. If $t_{m0}/\tau_R \sim 1$, the transport of NPs is mainly determined by their interaction with TLS; otherwise, it is mainly determined by elastic scattering. The signal detected in a relatively long sample at $t_{m0}/\tau_R \sim 1$ makes it possible to observe the specific feature related to the NP–TLS interaction against the background of elastic phonon scattering by lattice defects. Figure 1 shows an example of this behavior, where the $S(t)$ signals detected in the $Y_{2.7}Tb_{0.3}Al_5O_{12}$ sample ($L = 1$ cm, the low-level energy is $\Delta = 5.76$ K) by the bolometer at various temperatures are only caused by elastic interaction, $t_{m0}(T) < 4 \times 10^{-5}$ s. The specific feature induced by the NP–TLS interaction at times longer than 10^{-3} s is reflected on the trailing edges of the detected signals in the inset in the dependence $S(t) \propto t^{-1/2}$, which is characteristic of classical diffusion mode (1). The observa-

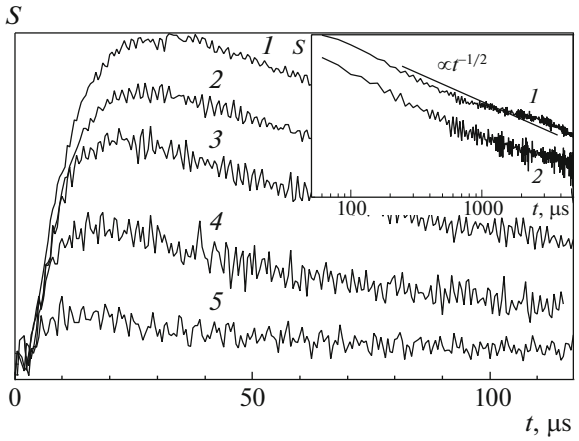

Fig. 1. NP signals in the $Y_{2.7}Tb_{0.3}Al_5O_{12}$ sample (L = 1 cm) at T = (*1*) 3.8, (*2*) 3.6, (*3*) 3.4, (*4*) 3, and (*5*) 2.7 K. (inset) Trailing edges on the log–log scale from [8]: T = (*1*) 3.8 and (*2*) 3 K.

tion of this interaction would be hampered in relatively short samples (L < 1 cm) in the absence of elastic scattering under ballistic propagation.

RESULTS

Figure 2 shows the $C(T)$ temperature dependences of solid-solution single crystals YAG:Re (Re = Er, Gd, Ho, Dy), TmAG:Er [10], GGG, and GGG:Er for a number of concentrations. In the low-temperature range, the dependence $C(T) \propto T^{-2}$ is seen to reflect the contribution of Schottky-like excitations to the total heat capacity against the background of the first excited Stark levels of ions Er^{3+} [10], Dy^{3+}, Gd^{3+}, Tm^{3+} [11], and Ho^{3+} [10]. The Er^{3+}, Dy^{3+}, and Gd^{3+} ions have the Kramers nature, which can give rise to the splitting of the ground level of an ion due to the local magnetic fields of the nearest neighbors in the absence of an external magnetic field.

The low-energy Stark level of the non-Kramers ion Ho^{3+} in YAG with an energy $\Delta \approx 5.7$ K was determined in [10]. In the TLS model, the contribution of this low-energy excitation to the total heat capacity in the temperature range under study (on the assumption that higher levels make an insignificant contribution) can be described by the expression

$$C(T) = R\frac{(\Delta/T)^2 e^{-\Delta/T}}{(1+e^{-\Delta/T})^2}, \qquad (3)$$

where R is the gas constant. For the $Y_{1.5}Ho_{1.5}Al_5O_{12}$ sample, the maximum in the $C(T)$ dependence in Fig. 2 is at $T_{max} = 0.417\Delta = 2.4$ K.

The situation is more complicated for the Kramers ions. The inset to Fig. 2 shows the concentration dependence of the splitting energy Δ of the ground level of the Er^{3+} ion in YAG, HoAG [10], and TmAG

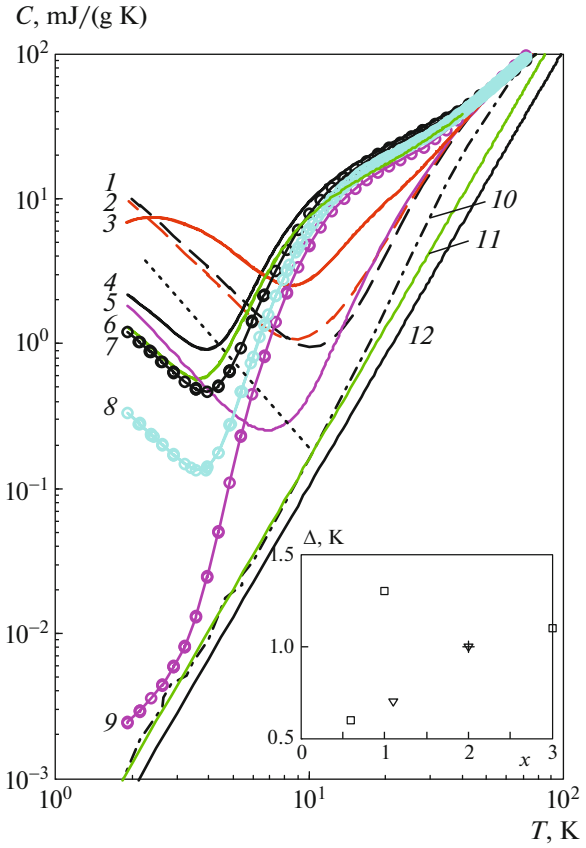

Fig. 2. Temperature dependences of the heat capacities of the following solid solution compositions: (*1*) GGG, (*2*) GGG:Er5%, (*3*) $Y_{1.5}Ho_{1.5}Al_5O_{12}$, (*4*) $Er_3Al_5O_{12}$, (*5*) $Y_2Dy_1Al_5O_{12}$, (*6*) $Y_2Er_1Al_5O_{12}$, (*7*) $Tm_1Er_2Al_5O_{12}$, (*8*) $Tm_2Er_1Al_5O_{12}$, (*9*) $Tm_3Al_5O_{12}$, and (*10*) $Y_3Al_5O_{12}$. Estimated phonon (Debye) contribution to the heat capacity of (*11*) $Er_1Y_2Al_5O_{12}$ and (*12*) $Er_3Al_5O_{12}$. (dotted line) Dependence $C(T) \propto T^{-2}$. (inset) Temperature dependence of Kramers doublet splitting energy Δ of the ground level of the Er^{3+} ion in the following RE garnet matrices [10, 11]: (□) YAG, (▽) TmAG, and (+) HoAG.

[11] in a zero external magnetic field. A wide heat capacity maximum, which is characteristic of the Kraers splitting, was detected for the $Y_2Er_1Al_5O_{12}$ sample at $T_{max} = 266 \pm 30$ mK when temperature was decreased in the range 93 mK–8 K [17].

As was shown in [5], the measure of efficiency of the interaction of NPs with TLS of various origins during the propagation of NPs in solid solution YAG:Re samples with various low-energy excitation concentrations are the NP range length (l_R) and time (τ_R) during interaction with TLS in addition to the time of detecting the signal maximum $t_m(T)$. If $t_{m0}/\tau_R \gg 1$ under experimental conditions, we have $t_m(L) \propto L$ and $\tau_R \propto T^{-5}/n$, where n is the RE ion concentration. The linear dependence $t_m(L) \propto L$ indicates an inelastic process during the NP–TLS interaction

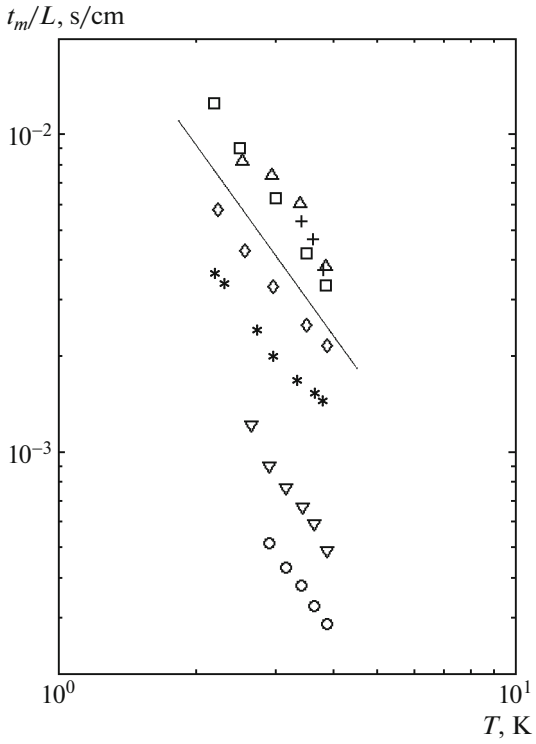

Fig. 3. Temperature dependences $t_m(T)$ normalized by sample length L for the following ER- and Ho-containing aluminum garnet solid solution single crystals: (□) $Er_3Al_5O_{12}$, $L = 0.22$ cm; (*)$Y_2ErAl_5O_{12}$, $L = 0.25$ cm; (○) $Tm_2ErAl_5O_{12}$, $L = 0.39$ cm; (▽) $TmEr_2Al_5O_{12}$, $L = 0.39$ cm; (◇) $Y_{1.5}Er_{1.5}Al_5O_{12}$, $L = 0.6$ cm; (△) $Y_{1.5}Ho_{1.5}Al_5O_{12}$, $L = 0.3$ cm; and (+) $Y_{2.5}Tb_{0.5}Al_5O_{12}$. (straight line) Dependence $t_m \propto T^{-2}$.

[15]. The character of NP transport in this case can be similar to the quasi-diffusion mode [16]: inelastic phonon decay processes because of lattice anharmonicity are possible against the background of intense elastic NP scattering in the diffusion mode when the phonon temperature (energy) increases. In this case, the $t_m(L)$ dependence is also close to a linear one [14].

Figure 3 shows the temperature dependences $t_m(T)/L$ normalized by the sample size. The dependences $t_m(T) \propto T^{-2}$ reflect the $C(T)$ dependences in the temperature range under study (see Fig. 2). When comparing the temperature dependences shown in Figs. 2 and 3, we can assume that the NP scattering at liquid-helium temperatures is also determined by low-energy excitations.

Salamatov [18] derived the following expression for the effective time of detecting the signal maximum, which reflects the relation between the kinetic characteristics and the heat capacity data at $C_{\text{tls}} \gg C_{\text{ph}}$ in samples of the same composition:

$$\frac{t_m(T)}{t_{m0}} \propto \frac{C_{\text{tls}}(T)}{C_{\text{ph}}(T)}, \tag{4}$$

where C_{tls} is the TLS-related heat capacity and C_{ph} is the phonon (Debye) heat capacity. t_{m0} is unambiguously related to the elastic scattering time, can be well calculated according to [13], and can be determined for any substitutional impurity concentration (as will be shown below in Fig. 8). The only quantity to be estimated in Eq. (3) is $C_{\text{ph}}(T)$. At low temperatures, we have

$$C_{\text{ph}}(T) = \frac{12\pi^4}{5} NR\left(\frac{T}{T_D}\right)^3, \tag{5}$$

where $N = 20$ is the number of atoms in the formula unit and T_D is the Debye temperature.

Equation (4) reflects the relation between the kinetic and thermodynamic characteristics of independent measurements. For example, the ratios of the right-hand to the left-hand side of this equation lie in the range 1–2.5 for the Er-containing YAG:Er and TmAG:Er solid solutions presented in Fig. 3 at $T =$ 3 K. The closeness to the equality of the right- and left-hand sides in Eq. (4) for relatively short samples can mean that equilibrium can be reached in the NP–TLS system in a sample of a certain length under the experimental conditions, namely, nonstationary heat pulse propagation. The determination of the conditions of equilibrium in the NP–TLS system in a nonstationary process requires additional studies and is beyond the scope of this work. Equation (4) does not contain kinetic characteristics τ_R and l_R, which reflect the specific features of the NP–TLS interaction that are caused by the nature of the paramagnetic ion in a solid solution, in an explicit form. Below, we give examples of independent estimation of l_R and τ_R in a number of solid solutions in RE garnets.

Figure 4 shows the bolometer-detected signals of $Y_{2.8}Er_{0.2}Al_5O_{12}$ and $Y_{2.8}Lu_{0.2}Al_5O_{12}$ samples of the same geometry ($L = 0.68$ cm) and concentration [19]. The insignificant difference between the RE ion masses in YAG:Re means the same level of elastic NP scattering and, hence, $D_0(T)$. The coincidence of the time dependences of the signal in the YAG:$Er_{0.2}$ and YAG:$Lu_{0.2}$ samples at $T = 2.91$ K allows us to determine $l_R = 0.68$ cm and $\tau_R = 10^{-5}$ s; according to Eq. (2), we have $l_R \approx \sqrt{D_0\tau_R}$.

l_R and τ_R in the $Y_{2.5}Tb_{0.5}Al_5O_{12}$ sample (Stark level of Tb^{3+} ion in YAG is $\Delta = 5.76$ K [20]) at $T = 3$ K were estimated using the results shown in Fig. 5. Unlike the data presented in Fig. 1, the NP–TLS interaction becomes predominant when the Tb^{3+} concentration increases and the major part of the NP energy concentrates in TLS. The estimation was carried out when the signal related to scattering by TLS disappears when the sample size decreases sequentially to 0.6 cm, and the

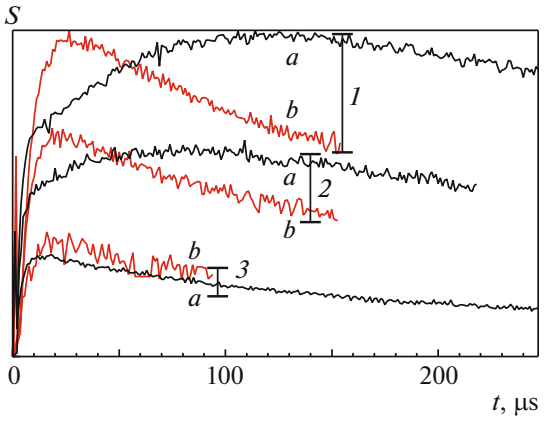

Fig. 4. NP signals in samples (*a*) $Y_{2.8}Er_{0.2}Al_5O_{12}$ and (*b*) $Y_{2.8}Lu_{0.2}Al_5O_{12}$ at $T = (1)$ 3.83, (*2*) 3.43, and (*3*) 2.91 K.

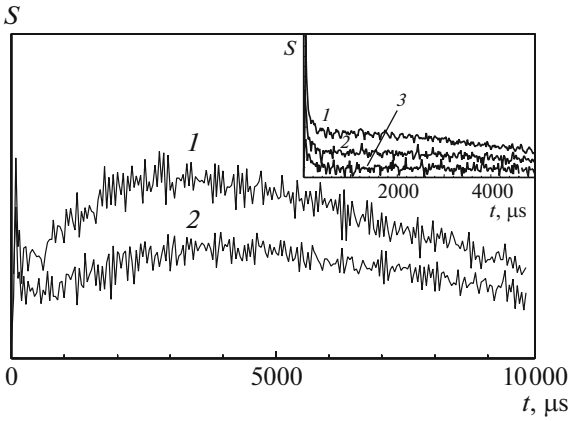

Fig. 5. NP signals in $Y_{2.5}Tb_{0.5}Al_5O_{12}$ sample with L = 0.75 cm at $T = (1)$ 3.8 and (*2*) 3.6 K [8]. (inset) The same for L = 0.6 cm and $T = (1)$ 3.8, (*2*) 3.6, and (*3*) 3.0 K.

estimated quantity was $\tau_R = 2.4 \times 10^{-5}$ s. In the $Y_{2.5}Er_{0.5}Al_5O_{12}$ sample, we have $\tau_R = 4 \times 10^{-5}$ s at T = 3 K; according to the dependence $\tau_R \propto T^{-5}$, it is lower by six times. The same is true of the $Y_{1.5}Ho_{1.5}Al_5O_{12}$ composition with a close value of the lower Stark level ($\Delta \approx 5.7$ K). The Er^{3+} ion exhibits similar activity in other solid state matrices, namely, yttrium monoaluminates [21], cation-vacancy garnets, and fluorite structures [22].

In Fig. 2, we presented the temperature dependences of $C(T)$ in impurity-free GGG and the GGG:Er5% sample. In both cases, low-energy contributions significantly contribute to the total heat capacity at liquid-helium temperatures.

Apart from the Kramers splitting of the ground level, GGG:Er5% also exhibits splitting of the $^4I_{15/2}$ multiplet of the Er^{3+} ion into eight Kramers doublets, and four lower doublets have energies of 0, 44.6, 63.3, and 90.6 K [23]. These energies are outside the available phonon energy range. Figure 6 shows the bolometer-detected signals of the GGG:Er5% sample with L = 0.4 cm and L = 0.2 cm, where the NP–TLS interaction may be neglected, at T = 3 K (inset). Here, we have $\tau_R = 1.6 \times 10^{-6}$ s, which is an order of magnitude lower than that in YAG:Er for the close composition $Y_{2.8}Er_{0.2}Al_5O_{12}$.

Figure 7 shows the NP signals in the impurity-free GGG and YAG matrix samples with L = 1 cm. The signals in both cases (diffusion maximum recording time is comparable with the ballistic signal time) are caused by elastic NP scattering by nonstoichiometric defects, Ga ↔ Gd substitution sites in GGG (less than 8%), and Al ↔ Y sites in YAG (less than 4%) in the octahedral environment of oxygen [24]. Thus, no interaction of NPs with the low-energy excitations in GGG occurs, in contrast to the heat capacity data (see Fig. 2). The low-energy excitations in GGG, which are induced by the spin multiplet $^8S_{7/2}$ of the Gd^{3+} ion (0, 1.5, 2.4, 4.4 K) were determined from the heat capacity data [21] and are within the temperature range under study. The absence of their interaction with heat phonon pulses under the experimental conditions was also observed in the YAG:Gd single crystals, which is indicated by the data shown in Fig. 8. At T = 3.4 K, the $t_{m0}(x)$ dependence normalized by L^2 illustrates elastic NP scattering in a number of YAG:Re solid solution samples. The same is true of the $Y_{2.4}Yb_{0.4}Gd_{0.2}Al_5O_{12}$ samples containing the Yb^{3+} Kramers ion, the ground level of which does to split in a zero external magnetic field and in other matrices [25].

In this case, the absence of interaction of NPs with the low-energy excitations in the Gd-containing solid solutions is associated with the half-filled 4*f* shell of

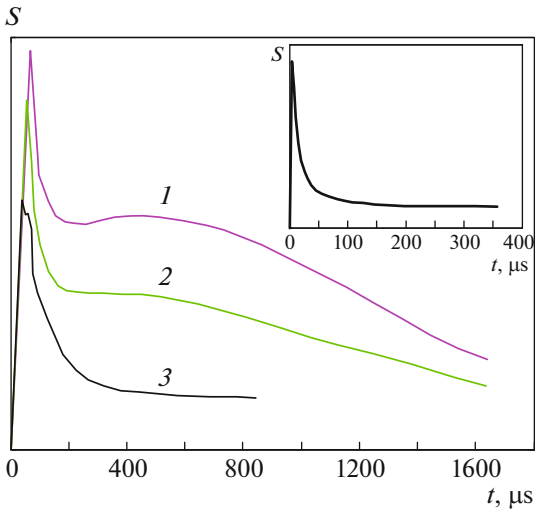

Fig. 6. NP signals in GGG:Er5% sample with L = 0.4 cm at $T = (1)$ 3.8, (*2*) 3.4, and (*3*) 2.93 K. (inset) Sample with L = 0.2 cm at T = 3.0 K.

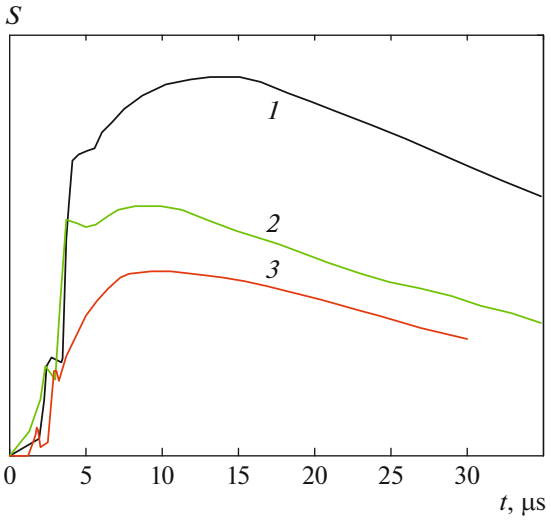

Fig. 7. NP signals in impurity-free YAG and GGG samples with $L = 1$ cm: (*1*) GGG, $T = 3.8$ K; (*2*) GGG, $T = 3.4$ K; and (*3*) YAG, $T = 3.4$ K.

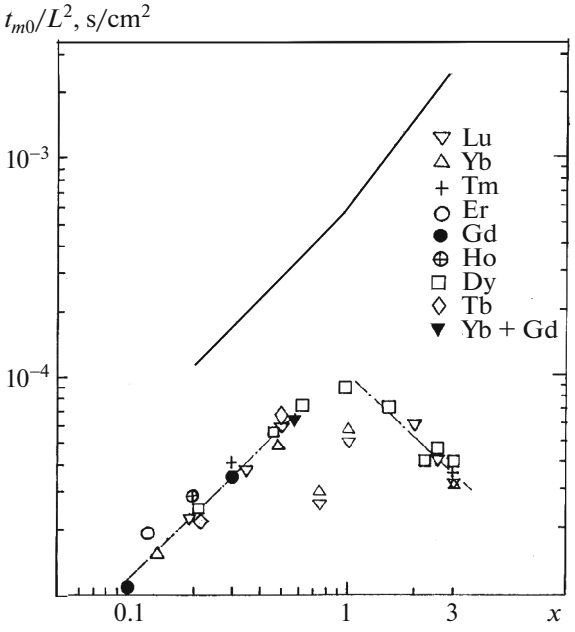

Fig. 8. Concentration dependences of the elastic NP scattering time ($T = 3.4$ K) normalized by L^2 in YAG:Re solid solutions. (solid line) Dependence $t_m(x)/L^2$ in YAG:Er.

the Gd^{3+} Kramers ion, and the orbital part of the moment is zero. It is the phonon modulation of the orbital electron motion that brings about interaction with TLS. However, this property of the Gd^{3+} ion, which restricts the coupling between lattice vibrations and spins, did not manifest itself in analogous experiments on gadolinium pentaphosphate glass [25].

Along with the data on fused quartz [26], Fig. 9 shows temperature dependences $t_m(T)$ for a number of pentaphosphate glasses ReP_5O_{14} based on the paramagnetic ions of the Ce series (Re = Ce, Sm, Gd). For glasses and glasslike materials (e.g., ferroelectric relaxors), we have $t_m(T) \propto T^n$, where $n > 4$, in the temperature range preceding a "plateau" in heat capacity. For fused quartz, we have $t_m(T) \propto T^5$ [26]. A weak contribution to the NP scattering, which is caused by interaction with low-energy excitations, is seen in Fig. 9 in pentaphosphate samples at close absolute values of t_m for fused quartz, SmP_5O_{14}, and CeP_5O_{14} when temperature decreases. The dependence for the Gd^{3+} ion is similar to those of Er-containing YAG solid solution single crystals.

The $C(T)$ dependence for the Dy^{3+} Kramers ion in YAG in Fig. 2 is shown only for the $Y_2Dy_1Al_5O_{12}$ sample with a ground state splitting energy $\Delta = 1.6$ K. The next doublet is separated from the ground state by more than 80 K and is outside the NP frequency range injected into the sample, as in the previous cases.

When discussing the experimental results until now, we restricted ourselves to a comparative analysis of the length and time of interaction (trapping) of NPs with TLS of a paramagnetic origin and left aside spin–lattice relaxation, which is responsible for exchange with the thermostat. This is allowable only when the spin–lattice relaxation time is comparable with or longer than the characteristic experiment time. The spin–lattice relaxation time for the Kramers ions Er^{3+}, Tb^{3+} [27], and Gd^{3+} [28] is more than 10^{-3} for an average temperature $T = 3$ K of measuring the transport characteristics. For the Dy^{3+} ion, this time is 10^{-9}–10^{-7} s [27, 29], which is much shorter than τ_0 and τ_R. Such a rapid relaxation hinders the possibility of accumulation and additional trapping of NPs in a sample. This result for the Dy^{3+} ion in YAG is reflected on the data in Fig. 8, where the results obtained for the entire YAG:Dy concentration range lie on the dependence that characterizes elastic NP scattering. However, the NP–TLS interaction is inelastic, which can lead to a transformation of the phonon spectrum injected into a sample under the experimental conditions. The fact of a short spin–lattice relaxation time (shorter than τ_0) can exclude the possibility of observation of an ordering effect in the YAG:Dy structure at 25% Dy, "blurring" the specific feature detected in YAG:Re (Lu, Yb) [30, 31]. As follows from the results presented in Fig. 8, the Yb^{3+} Kramers ion in the YAG structure also exhibits only elastic scattering under the experimental conditions.

Thus, the temperature dependences of heat capacity $C(T)$ and the transport characteristics of thermal phonons in the solid solutions of RE garnets at liquid-helium temperatures are substantially determined by Schottky-like low-energy paramagnetic excitations. The low-temperature heat capacities of almost all

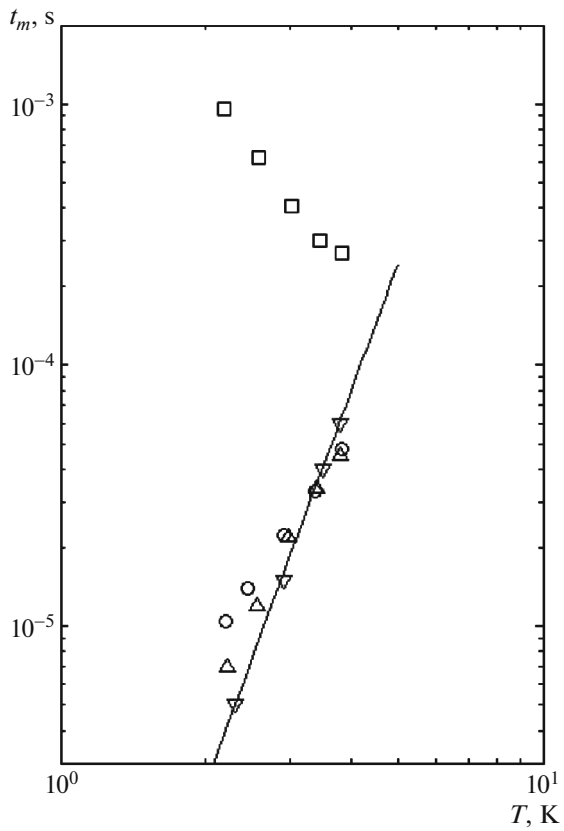

Fig. 9. Temperature dependences of the time of arrival of the NP signal maximum in the following RE pentaphosphate glasses and fused quartz: (○) SmP_5O_{14}, (□) GdP_5O_{14}, (△) CeP_5O_{14}, and (▽) SiO_2. (straight line) Dependence $t_m \propto T^5$.

paramagnetic ions of the Y series, namely, Gd^{3+}, Tb^{3+}, Dy^{3+}, Ho^{3+}, and Er^{3+} (except for Tm^{3+}, Lu^{3+}, Yb^{3+}), in a zero external magnetic field are higher than the phonon (Debye) heat capacity by 2–3 orders of magnitude. The efficiency of the NP–low-energy excitation interaction in the TLS model depends on the type of RE ion, the magnitude and the energy distribution of TLS, the ion momentum components, and the spin–lattice relaxation time in addition to the solid-solution concentration. For example, for NP–low-energy excitation interaction is absent for the Gd^{3+} Kramers ion in YAG:Gd solid solution single crystals and gallium–gadolinium garnet (GGG), and this interaction is also absent for the entire YAG:Dy solid solution range. This means that NP scattering is only determined by elastic scattering at the substitutional sites Y ↔ Gd and Y ↔ Dy. The absence of interaction in the NP–TLS system in the case of Gd^{3+} ion can be explained by the zeroth spin–orbit component of the magnetic moment of the ion. For the Dy^{3+} Kramers ion, the spin–orbit moment is nonzero; however, the spin–lattice relaxation is shorter than the elastic NP scattering time by 2–3 orders of magnitude according to different works. The low effective magnetic moment of the Yb^{3+} ion does not cause noticeable splitting of the ground level in a zero external magnetic field. Therefore, only elastic NP scattering is observed in Fig. 8 for the YAG:Gd and YAG:Gd,Yb compositions, and the Yb^{3+} ion does not contribute to the low-temperature heat capacity in a zero external magnetic field in a pentaphosphate YbP_5O_{14} single crystal [25]. Effective NP–TLS interaction is observed for the Er^{3+} ion. The nature of TLS for the Ho^{3+} and Tb^{3+} non-Kramers ions is represented by low Stark levels with energy $\Delta \approx 6$ K with respect to the ground level of the ion. The high efficiency (lower values of τ_R for the NP–TLS interaction) of the Er^{3+} ion, in contrast to Ho^{3+} and Tb^{3+} at close magnetic moments, is caused by TLS energy distribution over a spectrum, which is characteristic of the Kramers nature of the ion, where the local magnetic field at an ion site is determined by Er neighbors located at different distances.

FUNDING

This work was performed in terms of a state assignment and was supported in part by the Russian Foundation for Basic Research, project no. 18-07-00191.

REFERENCES

1. S. Nagata, H. Sasaki, K. Suzuki, et al., J. Phys. Chem. Sol. **62**, 1123 (2001).
2. K. Kamazawa, D. Louca, R. Morinaga, et al., Phys. Rev. B **78**, 064412 (2008).
3. E. V. Shevchenko, E. V. Charnaya, E. N. Khazanov, A. V. Taranov, and A. S. Bugaev, Phys. Solid State **59**, 733 (2017).
4. E. V. Shevchenko, E. V. Charnaya, M. K. Lee, et al., Phys. Lett. A **381**, 330 (2017).
5. E. I. Salamatov, A. V. Taranov, E. N. Khazanov, E. V. Charnaya and E. V. Shevchenko, J. Exp. Theor. Phys. **127**, 705 (2018).
6. A. Abragam and B. Bleaney, *Electron Paramagnetic Resonance of Transition Ions* (Oxford Univ., London, 1970), Vol. 1.
7. V. M. Mikushev and E. V. Charnaya, *Nuclear Magnetic Resonance in Solids* (SPb. Univ., St. Petersburg, 1995) [in Russian].
8. E. N. Khazanov, A. V. Taranov, E. V. Shevchenko, and E. V. Charnaya, J. Exp. Theor. Phys. **121**, 48 (2015).
9. A. A. Kaminskii, *Laser Crystals* (Nauka, Moscow, 1975) [in Russian].
10. E. V. Shevchenko, E. V. Charnaya, E. N. Khazanov, et al., J. Alloys Compd. **717**, 183 (2017).
11. E. V. Charnaya, E. V. Shevchenko, E. N. Khazanov, A. V. Taranov and A. M. Ulyashev, J. Commun. Technol. Electron. **64**, 811 (2019).
12. S. N. Ivanov, A. G. Kozorezov, A. V. Taranov, et al., Sov. Phys. JETP **73**, 880 (1991).

13. S. N. Ivanov, E. N. Khazanov, T. Paszkiewicz, et al., Z. Phys. B **99**, 535 (1996).
14. S. N. Ivanov and E. N. Khazanov, Sov. Phys. JETP **61**, 172 (1985).
15. I. B. Levinson, JETP Lett. **37**, 190 (1983).
16. D. V. Kazakovtsev and I. B. Levinson, JETP Lett. **27**, 181 (1978).
17. A. Kushino, Y. Aoki, N. Y. Yamasaki, et al., J. Appl. Phys. **90**, 5812 (2001).
18. E. I. Salamatov, Phys. Solid State **44**, 978 (2002).
19. S. N. Ivanov, E. N. Khazanov, A. G. Kozorezov, et al., Phys. Lett. A **159**, 279 (1991).
20. G. A. Slack and D. W. Oliver, Phys. Rev. B **4**, 592 (1971).
21. I. E. Lezova, O. V. Karban', A. V. Taranov, E. N. Khazanov, and E. V. Charnaya, J. Exp. Theor. Phys. **130**, 76 (2020).
22. S. N. Ivanov, A. G. Kozorezov, E. N. Khazanov, et al., Sov. Phys. JETP **73**, 880 (1991).
23. J. B. Gruber, D. K. Sardar, B. Zandi, et al., J. Appl. Phys. **93**, 3137 (2003).
24. Yu. I. Voron'ko and A. A. Sobol', Tr. FIAN **98**, 41 (1977).
25. I. E. Lezova, E. I. Salamatov, A. V. Taranov, E. N. Khazanov, E. V. Charnaya and E. V. Shevchenko, J. Exp. Theor. Phys. **129**, 849 (2019).
26. E. I. Salamatov, A. V. Taranov, and E. N. Khazanov, J. Exp. Theor. Phys. **121**, 267 (2015).
27. G. H. Larson and C. D. Jeffries, Phys. Rev. B **141**, 461 (1966).
28. V. A. Atsarkin, V. V. Demidov, G. A. Vasneva, et al., Phys. Rev. B **61**, R14944 (R) (2000).
29. J. C. Gill, Proc. Phys. Soc. **82**, 1066 (1963).
30. S. N. Ivanov, E. N. Khazanov, and A. V. Taranov, JETP Lett. **40**, 743 (1984).
31. P. Y. Efitsenko, E. N. Hazanov, S. N. Ivanov, et al., Phys. Lett. A **147**, 135 (1990).

Translated by K. Shakhlevich